WELDING RESEARCH

SUPPLEMENT TO THE WELDING JOURNAL, DECEMBER, 1985

Sponsored by the American Welding Society and the Welding Research Council

Readers are advised that all papers published in the *Welding Journal's* Research Supplement undergo Peer Review before publication for: 1) originality of the contribution; 2) technical value to the welding community; 3) prior publication of the material being reviewed; 4) proper credit to others working in the same area; and 5) justification of the conclusions based on the results.

The names of the more than 160 individuals serving on the AWS Peer Review Panel are published periodically. All are experts in their respective technical areas, and all are volunteers in the program.

Thermal Behavior of Austenitic-Ferritic Transition Joints Made by Friction Welding

Friction welding may reduce problems associated with joining dissimilar high pressure piping

BY K. G. K. MURTI AND S. SUNDARESAN

ABSTRACT. Transition joints between low-alloy and stainless steels in the superheater sections of steam-power boilers were made with friction welding. The joints were subjected to a variety of thermal conditions, including cycling and isothermal holds. The results indicate the suitability of friction welded joints for high-temperature, high-pressure applications. The microstructural changes occurring under the various test conditions have also been discussed.

Introduction

For purposes of economy, fossil-fired power plants use low-alloy ferritic steel tubing wherever possible and the more oxidation-resistant austenitic stainless steels where temperatures are higher, *e.g.*, in the final stages of superheater and reheater sections. Transition welds between ferritic and austenitic tubing thus become necessary. Three types of welds have been utilized: fusion welds with austenitic filler materials, fusion welds with nickel-base filler materials and pressure welds.

The use of transition welds poses several problems, such as cyclic thermal stresses caused by expansion differentials, low oxidation resistance of the low-alloy steel, and the diffusion of carbon from the ferritic alloy across the interface. Additional factors based on operational conditions aggravate the problem. The temperature is high and fluctuates owing to shut-down and start-up, and the stresses are due not only to steam pressure, but also arise from bending and vibration under external loads.

The problem of transition welds has assumed greater significance in recent years with reports of a number of service failures in fossil-fired steam plants (Ref. 1). While most of these have been associated with the use of austenitic stainless steel filler materials, nickel-base welds and pressure welds also cause concern. Of the three, however, the nickel-base welds appear to have the most trouble-free record (Ref. 2).

The failures have invariably occurred in the HAZ of the ferritic component, adjacent to the weld interface. This is the zone from which carbon has migrated and where the thermal stresses arise. The proposed mechanisms of failure are chiefly based upon the occurrence of creep-type damage in the carbon-depleted, weakened zone, aided by the oxidation of the susceptible ferritic material and the fluctuating stresses.

The occurrence of at least some of the failures before the end of the expected service life of the tubing has highlighted the need for an improved dissimilar alloy weld. Several methods for minimizing failures have been proposed: closer matching of expansion coefficients (if necessary, by the use of "graded" transition joints or spool pieces); buttering, to minimize carbon migration; stabilization of the ferritic component with carbide formers (again to reduce carbon diffusion); and avoidance of bending stresses and vibration, etc. (Ref. 3).

It may, however, be argued that the use of spool pieces with an intermediate expansion coefficient may be expensive and may also aggravate the problem by presenting more welds for potential fail-

K. G. K. MURTI is with the Welding Research Institute, BHEL, Tiruchirapalli, India, and S. SUNDARESAN is Professor and Head, Department of Metallurgical Engineering, Regional Engineering College, Tiruchirapalli, India.

Table 1—Compositions and Properties of Parent Materials

Parent Material	Chemical Composition, Wt % C	Mn	Si	Cr	Mo	Ni	P	S	Mechanical Properties Notch Tensile Strength N/mm²	Hardness VHN
Low-alloy steel (normalized and tempered)	0.10	0.48	0.65	1.04	0.5	-	0.03	0.03	585	224
Stainless steel (solution-treated)	0.07	2.00	0.75	18.7	-	11.4	0.03	0.04	689	206

ure locations. The use of carbon-stabilizing elements in the ferritic steel is impractical and also perhaps not ultimately effective for long-time exposure. It is in this context that a change of welding process appears to be a possible alternative. Friction welding is particularly attractive, as it avoids the use of additional weld metal and the associated dilution problems. The weld thermal cycle is rapid and reproducible, and joint properties at least equal to those of the weaker parent material can be attained. It may thus be possible that friction welding is a comparable alternative, especially in view of the fact that none of the past or presently used techniques is free from failure (Ref. 4). Some earlier investigations (Refs. 5, 6) have been concerned with the possible use of friction welding for high-temperature high-pressure application. The work reported in this paper is an attempt to assess the suitability of friction welding for making transition joints for steam power service.

Experimental Work

Materials

The low-alloy steel and the austenitic stainless steel used in the investigation are those employed in the platen superheater region (typical operating temperature 510°C/950°F) of steam power boilers. Their compositions and mechanical properties are indicated in Table 1. The parent materials were tubes with a 51 mm (2 in.) OD and a 7.1 mm (0.28 in.) wall thickness.

Equipment

A KUKA 20 kW continuous drive friction welding machine capable of 150 kN maximum load was used in the experiments. The machine has provision for four individual speed settings and for stepless adjustment of friction pressure, friction time, forging pressure, feed rate, brake delay time, upset delay time and upsetting time.

Variable Optimization

The welding variables most suited to the joining of the two steels were first determined in an earlier part of work reported elsewhere (Ref. 7). Variable optimization was carried out using the 2^3 factorial design of experiments. The three factors chosen were friction pressure, friction time and forging pressure, which are generally considered to be the variables controlling quality in friction welding. Notch tensile strength was taken as the criterion for evaluating weld quality. The optimum welding conditions and the corresponding strength of the joint are listed in Table 2.

Strips taken from the welded joints prepared under the optimized conditions of Table 2 were used for evaluating the performance of the transition welds in a variety of high temperature situations. While the ultimate objective was to estimate joint behavior under conditions closely simulating steam power service, fundamental studies were also initially made to investigate the effect of simple thermal exposure and thermal cycling.

Thermal Exposure Studies

Transverse strips from the welded joints were exposed at a constant temperature of 500°C (932°F) for periods of up to 125 h. After thermal exposure, the joints were observed metallographically. A hardness survey was also carried out for studying the effects of thermal exposure.

Thermal Cycling without Stress

A simplified thermal cycling procedure, similar to that described by Phillips and Reeves (Ref. 6), was employed, in which transverse strips from the welded joints were subjected to heating-cooling cycles without the application of stress. The limiting temperatures were selected to be 600° and 340°C (1112° and 644°F). The former is above the anticipated service temperature of 510°C (950°F), so that the phenomena occurring could be accelerated. The lower limit is typical of temperatures during boiler shutdown. Figure 1 shows a typical temperature record of the thermal cycles imposed, the temperature being registered at the weld interface with a thermocouple. Samples that had undergone 250 and 3000 cycles between these temperatures were subsequently evaluated for studying the changes due to simple thermal cycling.

A resistance heating transformer was used to pass current directly through the specimen for rapid heating. A time-switching programmer was connected to the primary so that it could be left to operate continuously on its own for long

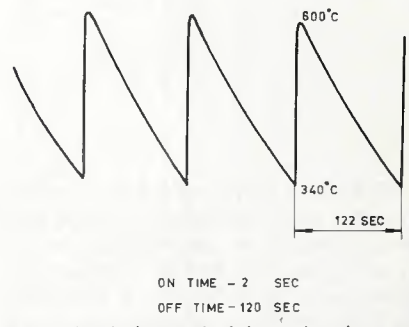

Fig. 1 — Typical record of thermal cycle

Fig. 2 — As-welded, etched in aqua-regia, weld interface indicated by arrow (200X)

Table 2—Optimum Welding Conditions and Joint Strength

Friction Pressure N/mm²	Friction Time Sec	Forging Pressure N/mm²	Rotational Speed RPM	Upsetting Time Sec	Notch Tensile Strength[a] N/mm²
32	13	88	1125	4.0	761

[a]Average of three trials.

durations with only occasional inspection. The specimen was allowed to move on heating and cooling by coupling its ends to the transformer secondary through flexible copper connections.

Stress-rupture Studies

Transition weld failures essentially have their origin in creep processes, and the occurrence of the failures in the carbon-depleted zone is to be attributed to its low creep strength. The stress-rupture test is hence an obvious route for assessing joint performance.

For accelerating high temperature tests, two basic possibilities exist: increasing the stress at operating temperature or increasing the temperature at operating stress. It has been argued that for Cr-Mo steels the over-temperature approach is to be preferred (Ref. 8). Keeping in view the typical operating temperature of 510°C (950°F) and design stress of 77 N/mm^2 (11,165 psi) for the ferritic steel, the stress-rupture tests were conducted at two temperature levels, 650° and 600°C (1202° and 1112°F), and three stress levels, 120, 90 and 60 N/mm^2 (17,400, 13,050 and 8700 psi). The results were plotted in terms of stress vs. rupture life. The predicted behavior for the operating conditions was then obtained using an appropriate time-temperature parameter (Ref. 9).

Thermal Cycling under Stress

In an operating steam plant, the stresses due to temperature variations during shutdown/start-up play a significant role in transition weld failures. It is well known that austenitic stainless steels have a thermal expansion coefficient much greater than that of ferritic low-alloy steels. For assessing the suitability of the joints for steam power service, the test procedure should hence incorporate temperature cycling among other service-simulating conditions.

A simplified accelerated test developed by Klueh, *et al.* (Ref. 10), was employed. Strips 127 × 12.7 × 4.5 mm (5 × 0.5 × 0.18 in.) taken from the welded joints were loaded with a set screw in a three-point bending fixture. The specimens under load were cycled between room temperature and 650°C (1202°F). Four stress levels were employed corresponding to 69, 138, 207 and 300 N/mm^2 (10,005, 20,010, 30,015 and 43,500 psi) at room temperature. A box-type furnace was used to heat the entire fixture to 650°C (1202°F). This temperature was maintained for 20 h, after which the fixture was removed from the furnace and air cooled to room temperature in about 2 h. The cycling was repeated by re-inserting the fixture into the furnace. Over each weekend, the specimens remained in the furnace for 48 h. After the specimens had been exposed to 24 cycles, they were removed from the test fixture and analyzed metallographically and with hardness measurements. In this treatment, the sample remains at 650°C (1202°F) for a total duration of 592 h. In terms of the Larson-Miller parameter, this simulates 6.9×10^6 h at the operating temperature of 510°C (950°F).

Results and Discussion

As-welded Condition

The welded joints produced under the statistically optimized parameters had notch tensile strength values which were consistently higher than those for the parent materials (see Tables 1 and 2).

The microstructures in the as-welded condition are shown in Figs. 2 and 3, respectively. In Fig. 2, the formation of a layer on the stainless steel side of the original interface may be seen. The layer is continuous and has a nearly uniform width of about 50 microns. The layer does not respond to a nital etch – Fig. 3. The deformed grain structure on the stainless steel side is characteristic of friction welds in this material.

The parent metal on the low-alloy steel side originally had the ferrite and pearlite structure of normalized low-carbon steels. As one moves towards the weld, there is a gradual suppression of proeutectoid ferrite and an increase in the formation of a fine ferrite-carbide aggregate, because of the faster cooling. This continues right up to the interface (Fig. 3), where neither the proeutectoid constituent nor any acicular phase can be observed. The interface is quite sharply defined and no layer formation is visible.

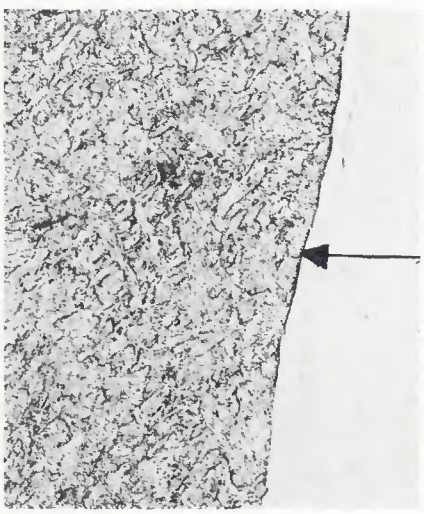

Fig. 3 – As-welded, etched in nital, weld interface indicated by arrow (200X) (stainless steel not attacked by nital)

Aging at 500°C

On the stainless steel side, the deformed grains next to the interface have recrystallized and grown on aging 125 h at 500°C (932°F) – Fig. 4. The interface layer appears to have grown to nearly twice its as-welded width, but on closer examination it may be observed that the 500°C (932°F) aging has led to the formation of an additional layer on the ferritic steel side of the original interface. The combined width of the layers varies from 100–120 microns.

On the low-alloy steel side there is little change due to the exposure at 500°C (932°F), except a slight coarsening of the ferrite-carbide aggregate – Fig. 5. There is no reduction in carbon content close to the weld. However, at the interface itself a dark-etching layer has appeared which

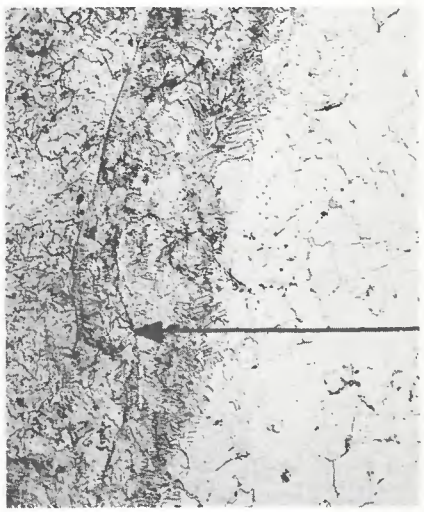

Fig. 4 – Specimen aged 125 h at 500°C, etched in aqua-regia, weld interface indicated by arrow (200X)

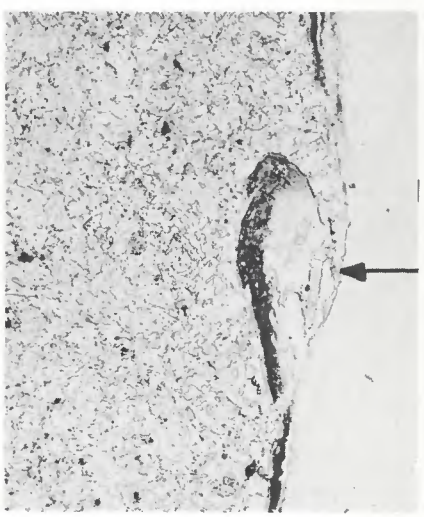

Fig. 5 – Specimen aged 125 h at 500°C, etched in nital, weld interface indicated by arrow (200X)

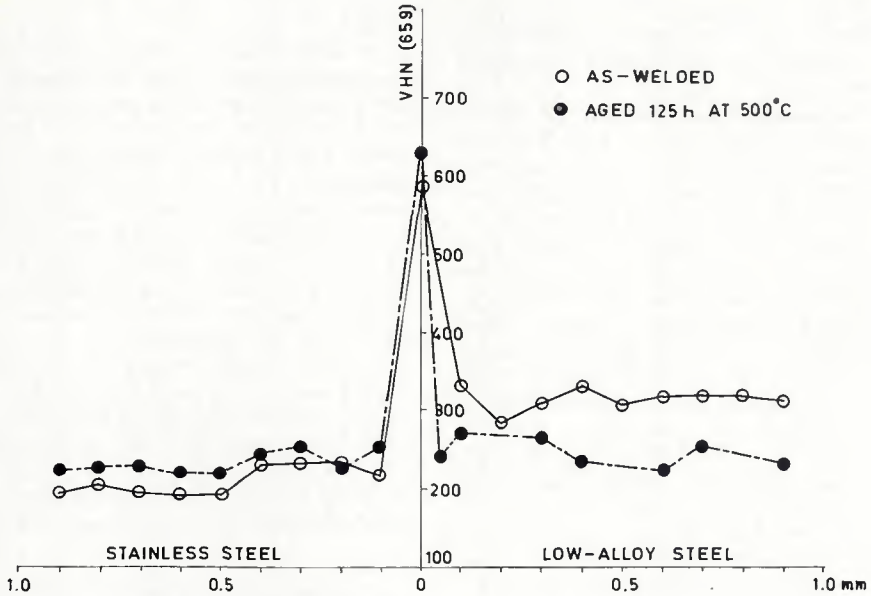

Fig. 6—Hardness survey across weld after thermal exposure

responds to a nital etch and is the same as the one seen in Fig. 4.

The hardness variations across the weld interface are plotted in Fig. 6 for a distance of 1 mm (0.04 in.) on either side. The reduction in hardness on the ferritic side upon aging at 500°C (932°F) is attributed to the coarsening effect seen in the microstructure. There is again no suggestion of any decarburization. At the interface, the hardness increases marginally over the as-welded value.

Thermal Cycling without External Load

The micrograph on the low-alloy steel side in the sample subjected to 250 cycles between 600° and 340°C (1112° and 644°F) is shown in Fig. 7. There are distinct features showing decarburization up to a distance of 0.2 mm (0.008 in.), on the average, from the weld interface. Farther away into the parent metal, the cycling has effected little change in the microstructure.

In the sample subjected to 3000 cycles (Fig. 8), the decarburized zone close to the interface is much less pronounced than that after 250 cycles. The formation of a dark-etching interface layer is clearly seen and it responds to a nital etch. This presumably is of the same nature as the one formed after aging for 125 h at 500°C (932°F). Indeed, the similarity between the microstructures in Fig. 5 and Fig. 8 is striking.

On the stainless steel side close to the interface, there is a coarse grain structure (Fig. 9—3000 cycles) which has obviously been preceded by recrystallization. Some

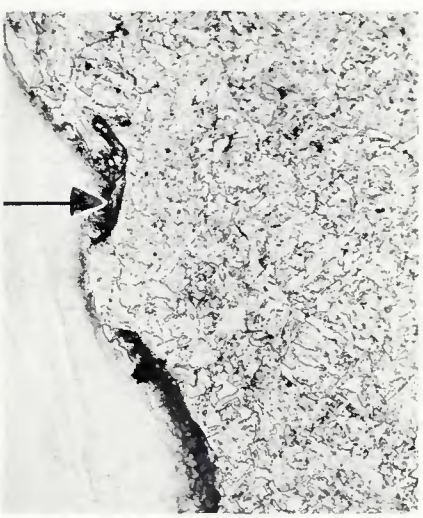

Fig. 8—Low-alloy steel after 3000 cycles of 600°-340°C, etched in nital, weld interface indicated by arrow (200X)

Fig. 9—Specimen after 3000 cycles of 600°-340°C, etched in aqua-regia, with weld interface indicated by arrow (200X)

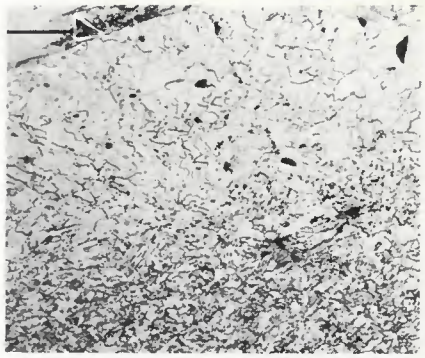

Fig. 7—Low-alloy steel side after 250 cycles of 600°-340°C, etched in nital, weld interface at top left indicated by arrow (200X)

grain boundary precipitation may also be seen, presumably arising from the carbon picked up during the early stages of cycling from the low-alloy steel. The interface layer etches very dark under aqua-regia, especially on the ferritic steel side.

These results show that thermal cycling is much more effective in promoting carbon migration than isothermal aging at 500°C (932°F). One reason is that the maximum temperature in thermal cycling was higher at 600°C (1112°F). The thermal stresses due to cycling might also play a role in enhancing the diffusion rate. The carbon depletion that occurs in 250 cycles is eliminated on prolonged cycling, probably by equalization as a result of diffusion of carbon from the farther regions in the ferritic side.

Figure 10 shows the hardness variation across the weld after thermal cycling. The occurrence of carbon depletion in the ferritic steel next to the interface is clearly demonstrated by the sharp hardness dip in this region in the sample cycled 250 times. At the interface, both cycled samples show a high hardness which is somewhat greater than in the as-welded condition.

We may now speculate upon the events occurring during welding and during subsequent thermal treatments. A layer forms at the interface on the austenitic steel side, but not on the ferritic steel side—Figs. 2 and 3. This layer has a hardness of 590 VHN. Since this sample has not received any post-weld heat treatment, the phases in this layer must form as a result of mixing of the two parent materials during welding. The only possibility, in view of the hardness and the rapid weld thermal cycle, appears to be martensite in which considerable alloy content is in solid solution. The compositions of the two steels are indicated in the Schaeffler diagram in Fig. 11. Alloying during welding must lead to an interface composition along the line PQ. It is thus reasonable to expect that the structure would be substantially, if not fully, martensitic.

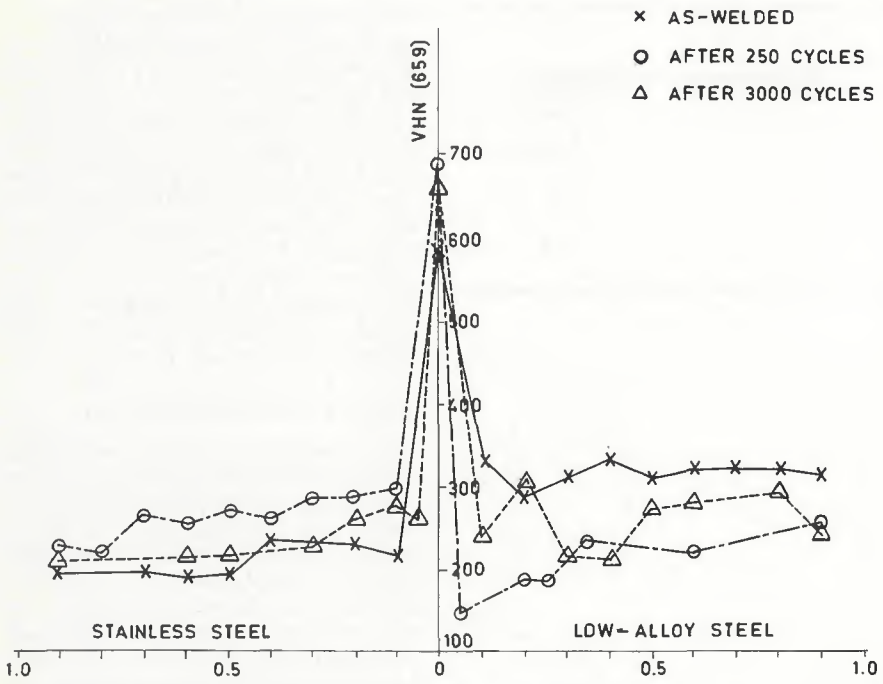

Fig. 10—Hardness survey across weld after thermal cycling (without load)

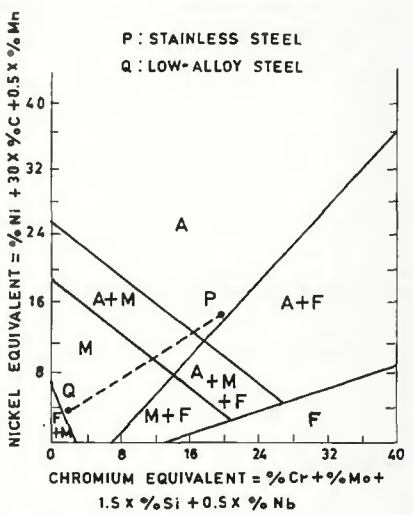

Fig. 11—Schaeffler diagram

The thermal treatments described so far have produced no appreciable change in the appearance of the above layer, but they have resulted in the formation of an additional layer, now on the ferritic steel side. This layer etches dark under nital and has a hardness that is somewhat higher than that of the layer on the austenitic steel side. In the as-welded condition (Fig. 3), there is no evidence of martensite in the ferritic steel even at the interface. The dark-etching layer cannot therefore be a consequence of martensite decomposition, as suggested by Wood (Ref. 11). The dark-etching layer forms (Figs. 5 and 8) even when there is apparently no carbon depletion in the low-alloy steel. Carbide precipitation by pick up of carbon may therefore also be ruled out. It is thus likely that the dark-etching layer comprises intermetallic phases for which formation is thermally activated. It is quite conceivable that mutual diffusion effects during the thermal treatments may lead to the formation of such compounds. This possibility is of course well known and has been suggested previously (Ref. 12).

Stress-rupture Testing

The results of the stress-rupture tests are shown in Fig. 12, which is a conventional plot of stress vs. rupture life for the two selected temperatures of 600° and 650°C (1112° and 1202°F). For predicting the behavior under the assumed service conditions (operating temperature 510°C/950°F and design stress 77 N/mm^2/11,165 psi), the time-temperature parameter used was of the form P = log t_r + CT = constant at constant stress, where P is the parameter, t_r the rupture life in hours and T the temperature in degrees Celsius. The constant C was evaluated at each stress level by measuring the separation between the isotherms on the conventional stress-rupture plots. As indicated in Table 3, the parameter P is then estimated for each stress level, as an average from the data obtained at both temperatures. In order to estimate the parameter P for the design stress of 77 N/mm^2 (11,165 psi), Fig. 13 has been plotted showing the variation of P as a function of stress. The value of the constant C for this stress level was evaluated as before from the stress-rupture plots. Substitution of these values of P and C enables an estimate of t_r to be made at 510°C (950°F). The calculation is indicated in Table 3, and shows that a rupture life of 6.4 × 10^5 h may be expected for the conditions of operation anticipated. This is well above the usual life expectancy of 100,000 h in such cases.

The results of metallographic examination of regions close to the fracture faces in a typical stress rupture sample are seen in Figs. 14 and 15. On the low-alloy steel side (Fig. 14), a decarburized zone is observed up to about 0.1 mm (0.004 in.), and this is where the creep rupture has occurred. On the stainless steel side (Fig. 15), a nital etch shows an interface band which comprises both the layers discussed previously. It is clear that rupture has occurred in the ferritic side away from the dark-etching layer.

Confirmation for the location of frac-

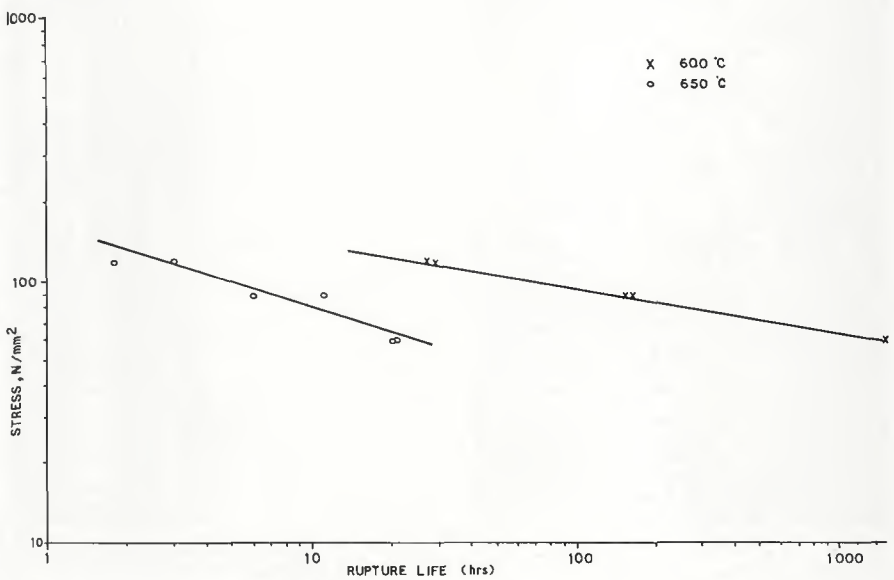

Fig. 12—Stress-rupture plots at 600° and 650°C

Table 3—Stress-rupture Data at 650° and 600°C

Stress N/mm²	Rupture Life, t_r (h) 650°C	600°C	$C = \frac{\Delta \log t_r}{\Delta T}$	P = (log t_r + CT) (average)
120	1.8	27	0.0213	14.25
	3.0	29		
90	6	151	0.0250	17.21
	11	153		
60	20	1500	0.0373	25.58
	21			

For design stress of 77 N/mm², C = 0.029 (from Fig. 12)
P = 20.6 (from Fig. 13).
Predicted rupture life at 510°C = 6.4×10^5 h (from P = log t_r + CT).

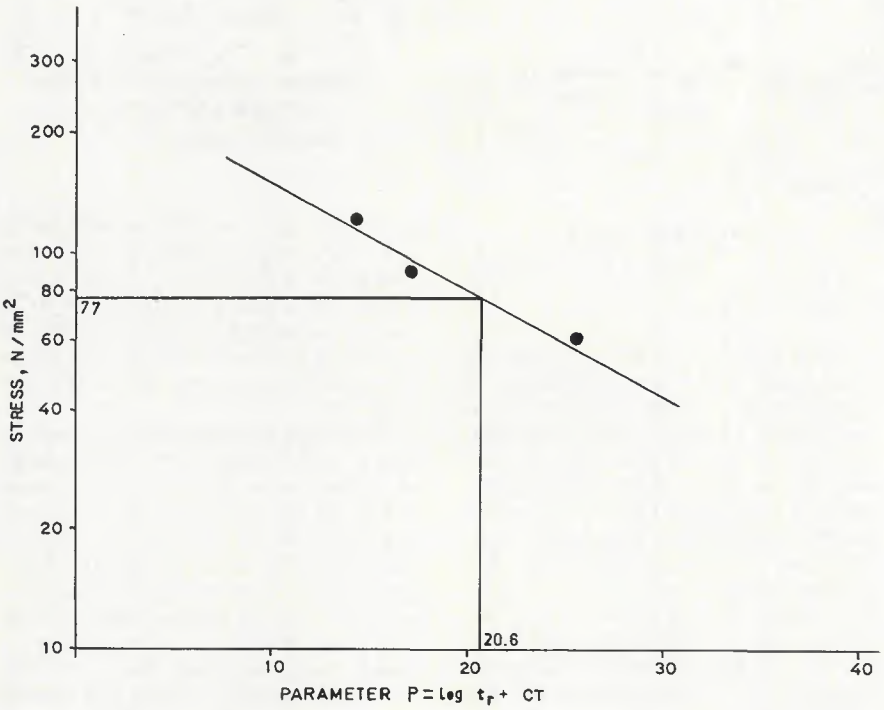

Fig. 13—Stress vs. time-temperature parameter (data from Table 3)

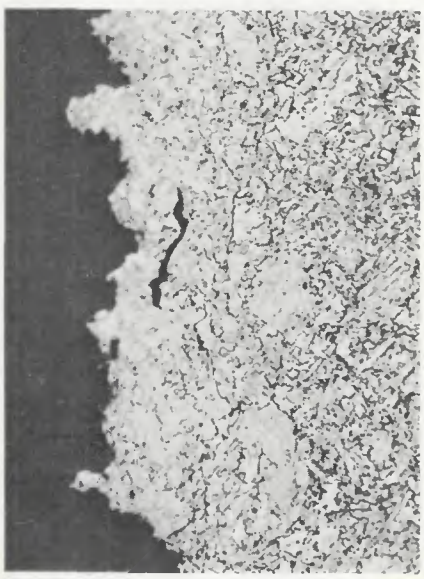

Fig. 14—Fracture region on low-alloy steel side after stress-rupture test, etched in nital (200X)

Fig. 15—Fracture region on stainless steel side after stress-rupture test, etched in nital (200X)

ture was also obtained from EDAX spectra on fracture faces investigated in the scanning electron microscope—Fig. 16. It can be clearly seen that there is hardly any evidence for the presence of nickel on either fracture face. The creep rupture has thus occurred in the decarburized zone in the ferritic steel too far away for nickel to diffuse from the austenitic steel. It is interesting to note that the creep behavior of the joints would thus depend on the properties of the carbon-denuded zone rather than on the nature of the interface phases.

Thermal Cycling with External Load

At none of the stress levels employed, including the highest (corresponding to 300 N/mm²/43,500 psi at room temperature), was any cracking observed on metallographic examination. The effective thermal exposure at 650°C (1202°F) amounts to 592 h and simulates 6.9×10^6 h at 510°C (950°F). In similar experiments by Klueh and co-workers on fusion welded transition joints, cracking was reported after 2300 h at 593°C (1099°F), which, according to the above parameter, is equivalent to 4×10^5 h at 510°C (950°F). The absence of cracking in our experiments would seem to establish that friction welds are at least as good as the fusion welds made with austenitic steel filler material.

Metallographically, the specimens tested at all the stress levels show similar features. On the low-alloy steel side there is no evidence for the dark-etching interface layer of intermetallics described earlier. However, there is considerable decarburization, and nearly pure ferrite grains are observed (Fig. 17) up to a distance of 4 mm (0.2 in.) from the interface. The absence of carbides also permits extensive grain growth in this region. Beyond 4 mm (0.16 in.), there is a gradual increase in carbon content and reduction in grain size.

On the stainless steel side, the original interface layer has grown to an average width of 0.15 mm (0.006 in.)—Fig. 18. The structure reveals growth of polygonal grains in this layer, which was not observed in the same region in any of the previous specimens. This layer is followed by a region about 0.25 mm (0.01 in.) wide which consists of a dense, dark-etching and fine-grained aggregate. Farther into the stainless steel, the austenitic grain structure with some grain boundary precipitation is observed—Fig. 19.

It is postulated that the long, effective exposure at the high temperature of 650°C (1202°F) has caused a large-scale migration of carbon from the ferritic side across the weld and across the interface layer. This has resulted in heavy carbide buildup in the stainless steel. These car-

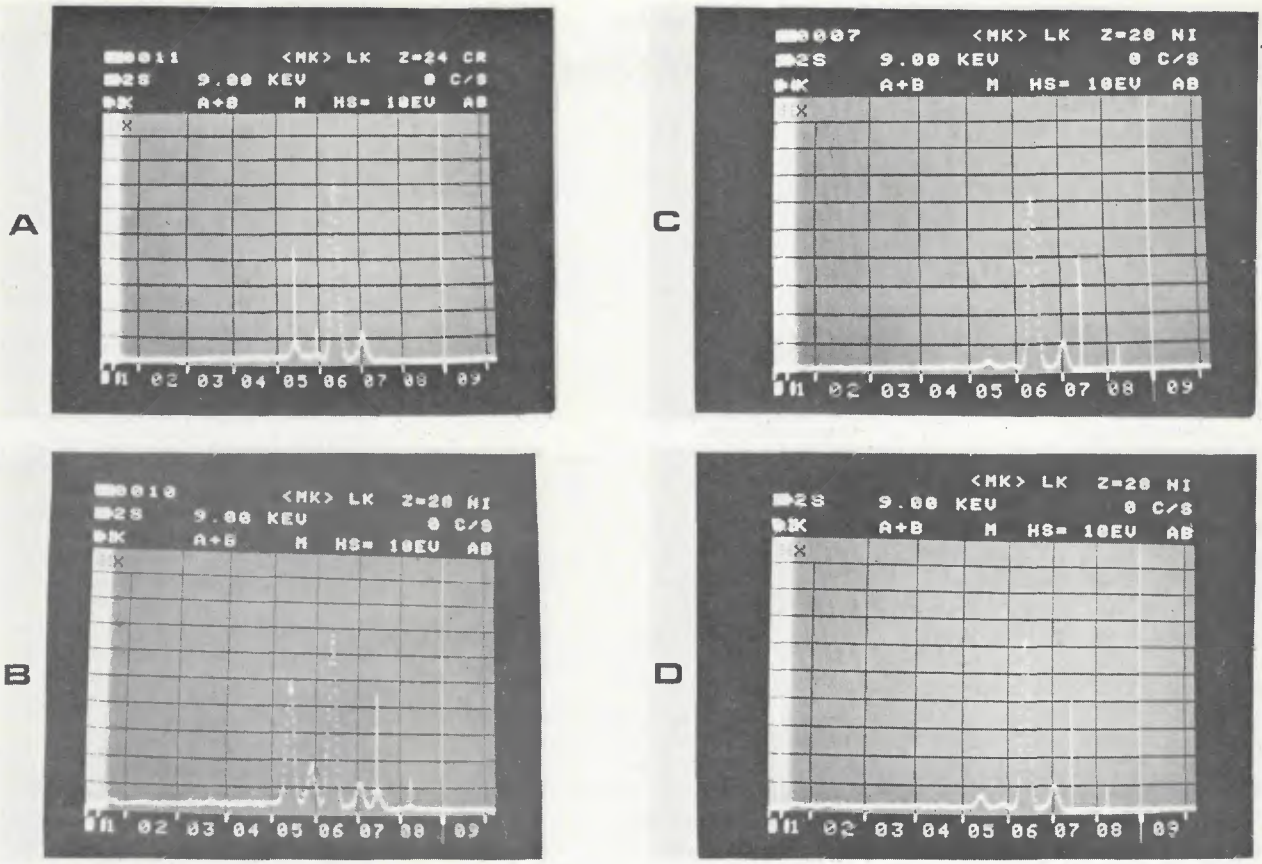

Fig. 16 — EDAX spectra from scanning electron microscope. (A) low-alloy steel base metal; (B) stainless steel base metal; (C) fracture surface on low-alloy steel side; (D) fracture surface on stainless steel side

bides, in conjunction with the hot deformation that would occur in this type of test, are responsible for the fine-grained dark-etching zone in Fig. 18. The formation of the carbides has also effectively hindered the occurrence of intermetallic phases observed after the thermal aging and cycling treatments described previously. In regions further away, the presence of carbides tapers off and the grain size is larger. These conclusions are borne out by the hardness variation plotted in Fig. 20. The interface hardness is lower than in the as-welded condition. This is presumably due to the absence of the dark-etching intermetallic layer that formed in some of the earlier treatments. The growth of polygonal grains in the

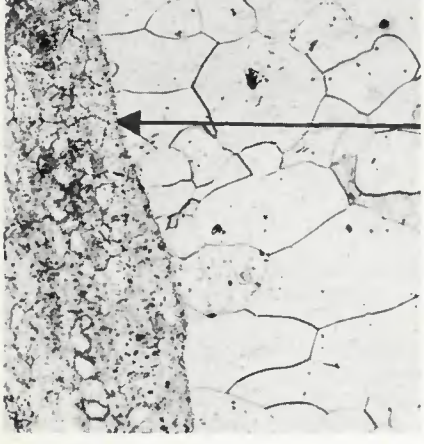

Fig. 17 — Low-alloy steel after thermal cycling under load, etched in aqua-regia, weld interface indicated by arrow (200X)

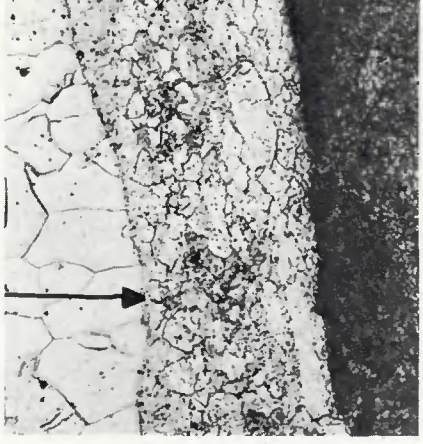

Fig. 18 — Interface region after thermal cycling under load, etched in aqua-regia, weld interface indicated by arrow (200X)

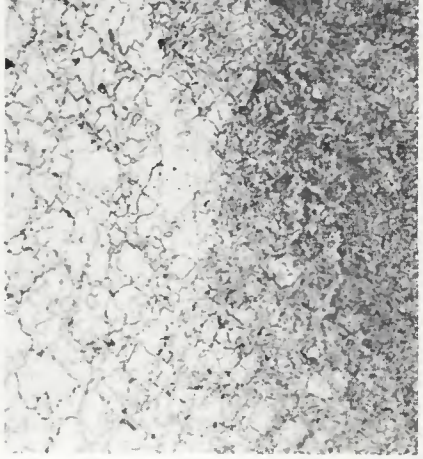

Fig. 19 — Stainless steel after thermal cycling under load, etched in aqua-regia (200X)

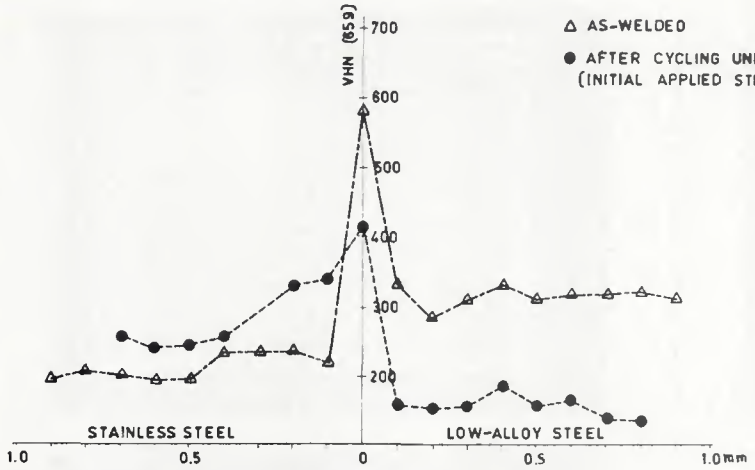

Fig. 20—Hardness survey after thermal cycling under stress

interface layer, in which the martensite formed during welding might have conceivably undergone tempering, may also contribute to the softening in this region. Immediately next to the interface on the stainless steel side, the hardness drops to about 360 VHN. This corresponds to the fine-grained zone consisting of dark-etching carbides in a matrix of austenite—Fig. 18. On the low-alloy steel side, the hardness quickly drops to values consistent with the observed decarburization.

It may be noted that in the previous thermal aging and cycling treatments (Figs. 6 and 10), the interface hardness rose to more than 600 VHN. It is reasonable to expect that this is due to the intermetallic phases that could form under these conditions in the absence of carbide buildup. Any softening as a result of the tempering of the as-welded interface martensite is effectively masked by the hardening due to the intermetallics.

Conclusions

1. The statistical optimization procedure for the welding conditions proved satisfactory in terms of joint properties which were even higher than those of the base metals.

2. During welding an interface layer forms on the stainless steel side which is presumably martensitic.

3. Thermal aging or cycling without an external load causes another interface layer to develop on the low-alloy steel side, and this is believed to consist of intermetallic phases.

4. Thermal cycling leads to carbon depletion in the ferritic steel more effectively than isothermal aging, but prolonged cycling tends to make the carbon distribution nearly uniform.

5. Stress-rupture studies indicate that, for the anticipated conditions of operation, the joints have a predicted life much longer than the usual life expectancy in such cases.

6. Creep failure occurs in the carbon-denuded zone in the low-alloy steel. The interface phases formed during welding and subsequent thermal treatments exert little influence on joint behavior under these conditions.

7. Thermal cycling tests under external load further reveal the suitability of friction welded austenitic-ferritic joints for high-temperature, high-pressure applications.

References

1. Klueh, R.L., and King, J.F. 1982. Austenitic stainless steel-ferritic steel weld joint failures. *Welding Journal* 61 (9):302-s to 311-s.

2. Dooley, R.B., Stephenson, G.G., Tinkler, M.J., Moles, M.D.C., and Westwood, H.J. 1982. Ontario Hydro experience with dissimilar metal welds in boiler tubing. *Welding Journal* 61 (2): 45-s to 49-s.

3. Lundin, C.D. 1982. Dissimilar metal welds-transition joints literature review, *Welding Journal* 61 (2): 58-s to 63-s.

4. American Electric Power Service Corporation 1978. Results of industry-wide survey on dissimilar metal weld performance. Annexure II.

5. Adams, D.F. 1969. Dissimilar metal joints for high temperature application. Proceedings of the Conference on Welding Dissimilar Metals, *Metal Construction & B.W.J.* 1 (12s):41-49.

6. Phillips, C., and Reeves, G.L. 1969. The development and evaluation of new methods of joining stainless steels to ferritic steels for high pressure/high temperature service. Ibid., 96-108.

7. Murti, K.G.K., and Sundaresan, S. 1983. Parameter optimisation in friction welding dissimilar materials. *Metal Construction* 15 (6):331-335.

8. Moles, M.D.C., Tinkler, M.J., and Westwood, H.J. 1981. Accelerated testing of three austenitic-ferritic superheater tube transition welds under simulated two shift conditions. *Metals Technology* 8 (4):121-129.

9. Clauss, F.J. 1969. *Engineer's Guide to High-Temperature Materials.* Addison-Wesley Publishing Co.

10. Klueh, R.L., King, J.F., and Griffith, J.L. 1983. A simple test for dissimilar-metal welds. *Welding Journal* 62 (6):154-s to 159-s.

11. Wood, D. 1969. Transition joints for high temperature service. Discussion, Proceedings of the Conference on Welding Dissimilar Metals, *Metal Construction & B.W.J.* 1 (12s):134.

12. Eaton, N.F., and Glossop, B.A. 1969. The welding of dissimilar creep-resisting ferritic steels. Ibid., 6-10.

WRC Bulletin 306
July 1985

PVRC Flanged Joint User Experience Survey
By J. R. Payne

Over 180 completed questionnaires were received from a distribution list of 295 flanged joint users. The results of the survey provided guidance in establishing research needs and priorities for flanged joint improvement programs.

The survey and the publication of the report were sponsored by the Task Group on Gasket Testing of the Subcommittee on Bolted Flanges of the Pressure Vessel Research Committee.

The price of WRC Bulletin 306 is $14.00 per copy, plus $5.00 for postage and handling. Orders should be sent with payment to the Welding Research Council, Rm. 1301, 345 E. 47th St., New York, NY 10017.